Pergamon

Int. J. Solids Structures Vol. 33, No. 26, pp. 3795–3812, 1996

0020-7683/96 $15.00 + .00

0020-7683(95)00214-6

MICROMECHANICAL ANALYSIS OF FIBER FRACTURE IN UNIDIRECTIONAL COMPOSITE MATERIALS

SCOTT W. CASE and KENNETH L. REIFSNIDER

Materials Response Group, Department of Engineering Science and Mechanics, Virginia Polytechnic Institute and State University, Blacksburg, VA 24061-0219, U.S.A.

(*Received* 16 *May* 1995; *in revised form* 27 *August* 1995)

Abstract In this paper, the problem of a penny-shaped crack in the center of multiple concentric cylinders is considered. By making appropriate choices for the stress functions in each of the constituents and making the standard assumptions of linear elasticity, it is possible to reduce the problem to the solution of a Fredholm integral equation of the second kind which may be solved numerically. This solution is used in conjunction with a geometry approximation to model the stress concentrations due to a broken fiber in a unidirectional composite material. The results suggest that models of such a shear lag may be missing important features of the stress state including surrounding broken fibers in composite materials. Copyright © 1996 Elsevier Science Ltd.

1. INTRODUCTION

The redistribution of stresses in bodies caused by the presence of a crack is one of the essential features that should be incorporated into an analysis of the strength of structures that contain such flaws (Paris and Sih, 1964). In particular, it is the high stresses in the vicinity of the crack tip that are of greatest importance—it is this region in which crack growth takes place. Griffith (1920) first put forward a theory for failure of brittle materials based on the presence of these defects. The fundamental concept of his theory is that the boundaries of a solid surrounding a crack possess a surface tension and that when a crack grows, the decrease in strain energy is balanced by the increase in the potential energy due to this surface tension. His analysis considered the case of a through-the-thickness crack in a thin plate—a two-dimensional problem. As noted by Paris and Sih (1964), in practical applications of those results, it must be remembered that all bodies are really three-dimensional. However, finding exact mathematical solutions for three-dimensional problems is of great difficulty in all but the simplest cases. One such case is the problem of a circular disk-crack subjected to a variety of loading conditions—a "penny-shaped" crack.

Sneddon (1946) was among the first to consider the penny-shaped crack problem. His analysis concerned a crack created in the interior of an infinite elastic medium occupying the circle $r^2 = x^2 + y^2 = c^2$ in the plane $z = 0$. Sneddon was able to exact expressions for the stresses at any point in the body. In addition, he applied a Griffith-type criterion for the condition of crack growth.

Collins (1962) also considered the case of a penny-shaped crack subjected to shear as well as normal loading. His approach was based on the use of two harmonic potential functions to represent the stresses and displacements. To illustrate the solution procedure, Collins determined the solution for four different penny-shaped crack problems:

(i) the opening of the crack by a point force acting at an interior point of the infinite solid
(ii) two parallel cracks in an infinite solid
(iii) an infinite row of parallel cracks in an infinite solid
(iv) and a crack in a thick plate with stress-free faces.

In all cases except for (i) approximate solutions to the resulting integral equations are presented. Collins presented expressions for the work of the crack and the maximum displacement of the crack faces.

Keer (1964) was the first to consider non-symmetrical loading of the penny-shaped crack. He used cylindrical polar coordinates (r, θ, z) where the crack, with radius a, is given by $z = 0$, $0 \leqslant r \leqslant a$. The crack is assumed to be opened by an arbitrary distribution of normal pressure. The problems are solved using a stress function technique similar to that employed by Green and Zerna (1960). Having obtained the solution for the problem of a crack in an infinite medium being opened by a non-symmetrical normal pressure, Keer next considered two other problems: a crack symmetrically loaded within a stress-free, thick elastic plate and a crack embedded in a beam exposed to pure bending. In the case of the crack in a thick plate, Keer derived a Fredholm integral equation of the second kind for the solution. The resulting equation must be solved by iteration or numerically.

Smith *et al.* (1967) developed an expression for the stress intensity factor of a penny-shaped crack in an infinite elastic solid subjected to non-axisymmetric normal loading. Their analysis began as Keers (1964) did in assuming that, in the absence of body forces, the complete solution for a restricted class of problems in which the shear stresses on the plane $z = 0$ can be represented by a single harmonic function, $\phi(r, \theta, z)$. They also expressed the loading on the crack surface as a Fourier series. By considering the general solution in the vicinity of the crack tip, Smith *et al.* developed an expression for the stress intensity factor for the opening mode of fracture. Additionally, they showed that the state of stress becomes that of plane strain at the tip of a penny-shaped crack for any non-axisymmetric continuous distribution of loading on the crack surface. To illustrate the applicability of their results, Smith *et al.* considered two particular cases: that of two concentrated forces at equal radial distances on the crack surface and that of a penny-shaped crack in a large beam subjected to pure bending.

Guidera and Lardner (1975) used the Somigliana formula from dislocation theory to solve the problem of a crack whose deformation is caused by the action of prescribed tractions on the crack surface. They obtained expressions for the stress intensity factors for two cases of loading of the crack plane, normal and shear.

Lardner and Tupholme (1976) considered much the same problem as that considered by Guidera and Lardner—only for a hexagonal crystal. By appropriately replacing certain isotropic constants by the appropriate elastic constants for the hexagonal material, they were able to obtain the stress intensity factors for a penny-shaped crack in a hexagonal medium. The resulting integral equations for the hexagonal medium are the same as those solved by Guidera and Lardner for the isotropic case. Lardner and Tupholme arrived at the stress intensity factors by direct substitution into the previous results. Using the results from the previous study by Guidera and Lardner for a constant unidirectional shear traction, Lardner and Tupholme studied the effect of the anisotropy on the distribution of stress in the vicinity of the crack.

Each of the above solutions considered the radial dimension of the body (the direction perpendicular to the crack) to be infinite. Sneddon and Tait (1963) considered the case of a very long (taken to be infinite) cylinder containing a crack with the center of the crack lying on the axis of the cylinder with the plane of the crack perpendicular to that axis. They assumed that the cylindrical surface is free from shear and is supported in such a way that the radial component of the displacement vector vanishes on the surface. Such a situation would arise physically if the elastic cylinder were resting in a hollow cylinder in a rigid body of exactly the same radius, if the cylinder were then deformed by the application of a known pressure to the surfaces of the crack. Sneddon and Tait presented the derivation of two solutions to the problem: one based on an integral-type solution and the other based on a series-type solution. The second is simpler, although it cannot be generalized to cover the case in which the cylinder surface is free from stress. Sneddon and Tait obtained an approximate solution for the case in which the crack is opened by a constant pressure.

Each of the problems considered previously has dealt with a penny shaped crack in a homogeneous material. Dhaliwal *et al.* (1979) considered the state of stress in a long elastic cylinder with a concentric penny-shaped crack, bonded to an infinite elastic medium. They

assumed the crack to be opened by an internal pressure and that the plane of the crack was perpendicular to the axis of the cylinder, and allowed the elastic constants of the cylinder and the semi-infinite medium to be different. They then reduced the problem to the solution of a Fredholm integral equation of the second kind and obtained closed-form expressions for the stress intensity factor and the crack energy.

The ability to include multiple constituents is of particular interest in the case of composite materials. For continuous fiber reinforced polymeric composite materials, the tensile strength is controlled by the stress distributions surrounding fiber fractures [Gao *et al.* (1992)]. In particular, the stress concentrations in fibers adjacent to the fractured ones and the distance over which the perturbed stress field acts (the *ineffective length*) are required for tensile strength predictions such as that presented by Batdorf (1982). Rosen (1964) was one of the first to study the stress redistribution which occurs in the vicinity of a fiber fracture in a unidirectional composite material. His analysis (a shear lag model) assumed that the fibers support only tensile loading, the matrix supports (and transmits) only shear loading, and that the shear transfer between the broken fiber and adjacent fibers is limited to the matrix between those fibers. Whitney and Drzal (1987) attempted to include normal loading in the matrix with their assumed stress function in the study of the stress distribution surrounding an isolated broken fiber.

In this paper, an analytical model is developed which provides an approximate stress state in the region surrounding a fiber fracture in a unidirectional composite material. The stress state is approximate in that the adjacent fibers have been smeared together to form a ring, making the resulting problem axisymmetric. Using a linear superposition technique in conjunction with a fiber discount analysis such as that suggested by Case *et al.* (1995), it is possible to determine the stress state in the neighborhood of multiple fiber fractures. This stress state may then be used in strength prediction models such as that described by Batdorf (1982) to arrive at the desired macrolevel strength predictions.

2. BASIC EQUATIONS AND THEIR SOLUTION

The present analysis is an extension of that employed by Dhaliwal *et al.* (1979) with modifications made to the potential functions to allow the body to include any number of concentric cylinder elements. We begin by considering the problem of a penny-shaped crack of radius r_c in an infinitely long elastic cylinder of radius r_1. This cylinder is surround by $N-1$ concentric elastic cylinders of radius r_i ($i = 2, N-1$), as shown in Fig. 1. The crack surface ($0 \leqslant r < r_c$) is subjected to a prescribed normal loading. The assumption of perfect bonding requires continuity of displacements and tractions at each interface ($r = r_1, r_2, \ldots r_{N-1}$). Since the geometry of the problem is symmetric about the plane $z = 0$, the problem reduces to a mixed boundary value problem for the region $z \geqslant 0$, $r \geqslant 0$. By assuming appropriate solutions for the regions of interest, the problem is reduced to the solution of a Fredholm integral equation of the second kind. This equation may be solved numerically. Once this solution has been obtained, it may be used to calculate the stress and displacement components in each of the constituent materials. By using a geometry approximation, it is then possible to used these stresses to determine the stress concentrations in unidirectional composite materials due to a single fiber fracture.

For the case of axisymmetric loading and boundary conditions, the displacement vector $\mathbf{U}$ assumes the form $(u_r, 0, u_z)$ in a cylindrical coordinate system (r, θ, z). The equations of equilibrium in terms of displacement are given by

$$\mu\nabla\mathbf{U} + (\lambda+\mu)\nabla(\nabla\cdot\mathbf{U}) = 0 \tag{1}$$

The corresponding stresses are given by

$$\sigma_{rr}(r,z) = (\lambda+2\mu)\frac{\partial u_r}{\partial r} + \lambda\left(\frac{u_r}{r} + \frac{\partial u_z}{\partial z}\right)$$

$$\sigma_{zz}(r,z) = (\lambda+2\mu)\frac{\partial u_z}{\partial z} + \lambda\left(\frac{u_r}{r} + \frac{\partial u_r}{\partial r}\right)$$

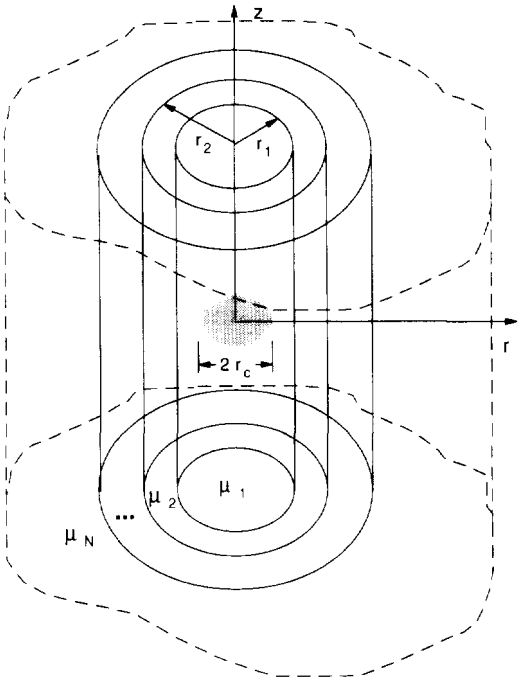

Fig. 1. Penny-shaped crack surrounded by multiple concentric cylinders having different elastic constants.

$$\sigma_{rz}(r,z) = \mu\left(\frac{\partial u_r}{\partial z} + \frac{\partial u_z}{\partial r}\right) \tag{2}$$

where λ and μ are Lamé's constants.

Following Dhaliwal *et al.* (1979), we may take the solution of the system of partial differential equations given by eqn (1) in the form of

$$u_r(r,z) = (1-2\nu)\frac{\partial \chi}{\partial r} + z\frac{\partial^2 \chi}{\partial r \partial z} + \frac{\partial \phi}{\partial r} + (3-4\nu)\psi - r\frac{\partial \psi}{\partial r}$$

$$u_z(r,z) = -2(1-\nu)\frac{\partial \chi}{\partial z} + z\frac{\partial^2 \chi}{\partial z^2} + \frac{\partial \phi}{\partial z} - r\frac{\partial \psi}{\partial z} \tag{3}$$

where ν is Poisson's ratio and the functions χ, ϕ, and ψ satisfy the following relations

$$\left(\frac{\partial^2}{\partial r^2} + \frac{1}{r}\frac{\partial}{\partial r} + \frac{\partial^2}{\partial z^2}\right)\chi = 0$$

$$\left(\frac{\partial^2}{\partial r^2} + \frac{1}{r}\frac{\partial}{\partial r} + \frac{\partial^2}{\partial z^2}\right)\phi = 0$$

$$\left(\frac{\partial^2}{\partial r^2} + \frac{1}{r}\frac{\partial}{\partial r} + \frac{\partial^2}{\partial z^2} - \frac{1}{r^2}\right)\psi = 0 \tag{4}$$

Solution of eqns (4) for the regions R_i, $1 \leqslant i \leqslant N$, are taken in the form of

$$\chi^{(1)}(r,z) = \int_0^\infty \frac{1}{\xi^2} F(\xi) J_0(\xi r)\, e^{-\xi z}\, d\xi$$

$$\phi^{(1)}(r,z) = \int_0^\infty \frac{1}{\xi} A(\xi)[I_0(\xi r)\cos(\xi z) - 1]\, d\xi, \quad (r,z) \in R_1$$

$$\psi^{(1)}(r,z) = \int_0^\infty B(\xi) I_1(\xi r)\cos(\xi z)\, d\xi \tag{5}$$

$$\chi^{(i)}(r,z) = 0$$

$$\phi^{(i)}(r,z) = \int_0^\infty \frac{1}{\xi}[C^{(i)}(\xi)K_0(\xi r) + E^{(i)}(\xi)I_0(\xi r)]\cos(\xi z)\, d\xi, \quad (r,z) \in R_i, \quad 2 \leqslant i \leqslant N-1$$

$$\psi^{(i)}(r,z) = \int_0^\infty [D^{(i)}(\xi)K_1(\xi r) + G^{(i)}(\xi)I_1(\xi r)]\cos(\xi z)\, d\xi \tag{6}$$

$$\chi^{(N)}(r,z) = 0$$

$$\phi^{(N)}(r,z) = \int_0^\infty \frac{1}{\xi} C^{(N)}(\xi)K_0(\xi r)\cos(\xi z)\, d\xi, \quad (r,z) \in R_N$$

$$\psi^{(N)}(r,z) = \int_0^\infty D^{(N)}(\xi)K_1(\xi r)\cos(\xi z)\, d\xi \tag{7}$$

where the superscript i ($i = 1, 2 \ldots N$) denote quantities for the regions R_i and $J_j(\xi r)$, $I_j(\xi r)$, and $K_j(\xi r)$ denote Bessel functions of the first kind and modified Bessel functions of the first and second kind, respectively, of orders j ($j = 0, 1$). From eqns (2), (3), (5)–(7), we obtain the following expressions for the stress and displacement components in the regions R_i, $i = 1, 2, \ldots N$:

$$u_r^{(1)} = \int_0^\infty \left[\frac{1}{\xi}(2\nu_1 - 1 + \xi z)F(\xi)J_1(\xi r)\, e^{-\xi z} + \{A(\xi)I_1(\xi r) + B(\xi)[4(1-\nu_1)I_1(\xi r) - \xi r I_0(\xi r)]\}\cos(\xi z)\right] d\xi \tag{8}$$

$$u_z^{(1)} = \int_0^\infty \left[\frac{1}{\xi}(2 - 2\nu_1 + \xi z)F(\xi)J_0(\xi r)\, e^{-\xi z} - \{A(\xi)I_0(\xi r) - \xi r B(\xi)I_1(\xi r)\}\sin(\xi z)\right] d\xi \tag{9}$$

$$\sigma_{rr}^{(1)} = \int_0^\infty 2\mu_1 \left[\left\{(\xi z - 1)J_0(\xi r) + (1 - 2\nu_1 - \xi z)\frac{1}{\xi r}J_1(\xi r)\right\}F(\xi)\, e^{-\xi z} - \frac{1}{r}\{A(\xi)[I_1(\xi r) - \xi r I_0(\xi r)] + B(\xi)[(4 - 4\nu_1 + \xi^2 r^2)I_1(\xi r) - (3 - 2\nu_1)\xi r I_0(\xi r)]\}\cos(\xi z)\right] d\xi \tag{10}$$

$$\sigma_{zz}^{(1)}(r,z) = -2\mu_1 \int_0^\infty [(1 + \xi z)F(\xi)J_0(\xi r)\, e^{-\xi z} + \xi\{A(\xi)I_0(\xi r) - B(\xi)[2\nu_1 I_0(\xi r) + \xi r I_1(\xi r)]\}\cos(\xi z)]\, d\xi \tag{11}$$

$$\sigma_{rz}^{(1)}(r,z) = -2\mu_1 \int_0^\infty [\xi z F(\xi) J_1(\xi r)\, e^{-\xi z} + \xi\{A(\xi) I_1(\xi r) + B(\xi)[2(1-\nu_1) I_1(\xi r) - \xi r I_0(\xi r)]\} \sin(\xi z)]\, d\xi \quad (12)$$

$$u_r^{(i)}(r,z) = \int_0^\infty \{-C^{(i)}(\xi) K_1(\xi r) + E^{(i)}(\xi) I_1(\xi r) + D^{(i)}(\xi)[4(1-\nu_i) K_1(\xi r) + \xi r K_0(\xi r)] + G^{(i)}(\xi)[4(1-\nu_i) I_1(\xi r) - \xi r I_0(\xi r)]\} \cos(\xi z)\, d\xi \quad (13)$$

$$u_z^{(i)}(r,z) = \int_0^\infty \{-C^{(i)}(\xi) K_0(\xi r) - E^{(i)}(\xi) I_0(\xi r) + D^{(i)}(\xi) \xi r K_1(\xi r) + G^{(i)}(\xi) \xi r I_1(\xi r)\} \sin(\xi z)\, d\xi \quad (14)$$

$$\sigma_{rr}^{(i)}(r,z) = \frac{2\mu_i}{r} \int_0^\infty \{C^{(i)}(\xi)[\xi r K_0(\xi r) + K_1(\xi r)] - D^{(i)}(\xi)[(4-4\nu_i+\xi^2 r^2) K_1(\xi r) + (3-2\nu_i)\xi r K_0(\xi r)] + E^{(i)}(\xi)[\xi r I_0(\xi r) - I_1(\xi r)] - G^{(i)}(\xi)[(4-4\nu_i+\xi^2 r^2) I_1(\xi r) - (3-2\nu_i)\xi r I_0(\xi r)]\} \cos(\xi z)\, d\xi \quad (15)$$

$$\sigma_{rz}^{(i)}(r,z) = 2\mu_i \int_0^\infty \xi\{C^{(i)}(\xi) K_1(\xi r) - D^{(i)}(\xi)[2(1-\nu_i) K_1(\xi r) + \xi r K_0(\xi r)] - E^{(i)}(\xi) I_1(\xi r) - G^{(i)}(\xi)[2(1-\nu_i) I_1(\xi r) + \xi r I_0(\xi r)]\} \sin(\xi z)\, d\xi \quad (16)$$

$$\sigma_{zz}^{(i)}(r,z) = -2\mu_i \int_0^\infty \xi\{C^{(i)}(\xi) K_0(\xi r) + D^{(i)}(\xi)[2\nu_i K_0(\xi r) - \xi r K_1(\xi r)] + E^{(i)}(\xi) I_1(\xi r) - G^{(i)}(\xi)[2\nu_i I_0(\xi r) + \xi r I_1(\xi r)]\} \cos(\xi z)\, d\xi \quad (17)$$

$$u_r^{(N)}(r,z) = \int_0^\infty \{-C^{(N)}(\xi) K_1(\xi r) + D^{(N)}(\xi)[4(1-\nu_N) K_1(\xi r) + \xi r K_0(\xi r)]\} \cos(\xi z)\, d\xi \quad (18)$$

$$u_z^{(N)}(r,z) = \int_0^\infty \{-C^{(N)}(\xi) K_0(\xi r) + D^{(N)}(\xi) \xi r K_1(\xi r)\} \sin(\xi z)\, d\xi \quad (19)$$

$$\sigma_{rr}^{(N)}(r,z) = \frac{2\mu_N}{r} \int_0^\infty \{C^{(N)}(\xi)[\xi r K_0(\xi r) + K_1(\xi r)] - D^{(N)}(\xi)[(4-4\nu_N+\xi^2 r^2) K_1(\xi r) + (3-2\nu_N)\xi r K_0(\xi r)]\} \cos(\xi z)\, d\xi \quad (20)$$

$$\sigma_{rz}^{(N)}(r,z) = 2\mu_N \int_0^\infty \xi\{C^{(N)}(\xi) K_1(\xi r) - D^{(N)}(\xi)[2(1-\nu_N) K_1(\xi r) + \xi r K_0(\xi r)]\} \sin(\xi z)\, d\xi \quad (21)$$

$$\sigma_{zz}^{(N)}(r,z) = -2\mu_N \int_0^\infty \xi\{C^{(N)}(\xi) K_0(\xi r) + D^{(N)}(\xi)[2\nu_N K_0(\xi r) - \xi r K_1(\xi r)]\} \cos(\xi z)\, d\xi \quad (22)$$

where μ_i and v_i denote the shear modulus and Poisson's ratio for the region R_i ($i = 1, 2, \ldots N$).

3. FORMULATION OF THE PROBLEM

The problem of a penny shaped-crack of radius r_c in a long elastic cylinder of radius $r_1 (r_1 > r_c)$ is considered. We assume that there is perfect bonding between each of the constituents. All of the materials are assumed to be homogeneous and isotropic. Since the geometry of the problem is symmetric about the crack plane, we consider a semi-infinite elastic cylinder subjected to the following boundary conditions:

$$\sigma_{zz}^{(1)}(r,0) = p(r), \quad 0 < r < r_c \tag{23}$$

$$u_z^{(1)}(r,z) = 0, \quad r_c < r < r_1 \tag{24}$$

$$\sigma_{rz}^{(1)}(r,0) = 0, \quad 0 < r < r_1 \tag{25}$$

$$u_z^{(i)}(r,z) = 0, \quad r_{i-1} < r < r_i \tag{26}$$

$$\sigma_{rz}^{(i)}(r,0) = 0, \quad r_{i-1} < r < r_i \tag{27}$$

The continuity conditions for displacements and tractions are given by

$$\begin{aligned} u_z^{(i)}(r_i,z) &= u_z^{(i+1)}(r_i,z) \\ u_r^{(i)}(r_i,z) &= u_r^{(i+1)}(r_i,z) \\ \sigma_{rr}^{(i)}(r_i,z) &= \sigma_{rr}^{(i+1)}(r_i,z) \\ \sigma_{rz}^{(i)}(r_i,z) &= \sigma_{rz}^{(i+1)}(r_i,z) \end{aligned} \tag{28}$$

4. REDUCTION OF THE PROBLEM TO THE SOLUTION OF A FREDHOLM INTEGRAL EQUATION OF THE SECOND KIND

Due to the functional forms chosen for χ, ϕ, and ψ in each of the constituents, it is apparent that the boundary conditions given by eqns (24)–(27) are identically satisfied by the stresses and displacements given in eqns (12), (14), (16), (19) and (21). Substituting eqns (11) and (9) into the boundary conditions given by eqns (23) and (24), we arrive at the following dual integral equations:

$$\int_0^\infty F(\xi)J_0(\xi r)\,\mathrm{d}\xi + \int_0^\infty \xi\{A(\xi)I_0(\xi r) - B(\xi)(2v_1 I_0(\xi r) + \xi r I_1(\xi r))\}\,\mathrm{d}\xi = \frac{-p(r)}{2\mu_1}$$

$$0 < r < r_c \tag{29}$$

$$\int_0^\infty \frac{1}{\xi} F(\xi)J_0(\xi r) = 0 \quad r_c < r < r_1 \tag{30}$$

Equation 30 is identically satisfied if the solution for $F(\xi)$ is taken as

$$F(\xi) = \xi \int_0^{r_c} h(t)\sin(\xi t)\,\mathrm{d}t \tag{31}$$

regardless of the form of $h(t)$.

Substituting eqn (31) into eqn (29), we see that the function $h(t)$ must satisfy

$$h(t)+\frac{2}{\pi}\int_0^\infty \xi\left\{[A(\xi)-2\nu_1 B(\xi)]\int_0^t \frac{rI_0(\xi r)\,dr}{\sqrt{(t^2-r^2)}}-\xi B(\xi)\int_0^t \frac{r^2 I_1(\xi r)\,dr}{\sqrt{(t^2-r^2)}}\right\}d\xi$$
$$=-\frac{1}{\pi\mu_1}\int_0^t \frac{rp(r)\,dr}{\sqrt{(t^2-r^2)}} \tag{32}$$

Making use of the fact that

$$\int_0^t \frac{rI_0(\xi r)\,d\xi}{\sqrt{(t^2-r^2)}}=\frac{\sinh(\xi t)}{\xi}$$
$$\int_0^t \frac{r^2 I_1(\xi r)\,d\xi}{\sqrt{(t^2-r^2)}}=\frac{\xi t\cosh(\xi t)-\sinh(\xi t)}{\xi^2}$$

and substituting into eqn (32) we find that

$$h(t)+\frac{2}{\pi}\int_0^\infty \{[A(\xi)-2\nu_1 B(\xi)]\sinh(\xi t)-(\xi t\cosh(\xi t)-\sinh(\xi t))B(\xi)\}\,d\xi$$
$$=-\frac{1}{\pi\mu_1}\int_0^t \frac{rp(r)\,dr}{\sqrt{(t^2-r^2)}} \tag{33}$$

Using the Fourier inversion theorem along with the boundary conditions given by eqns (28) and the stress and displacements given by eqns (8)–(10) and (12)–(16), we obtain the following relations for $r=r_1$:

$$-I_0(r_1 s)A(s)+r_1 sI_1(r_1 s)B(s)+K_0(r_1 s)C^{(2)}(s)-r_1 sK_1(r_1 s)D^{(2)}(s)$$
$$+I_0(r_1 s)E^{(2)}(s)-r_1 sI_1(r_1 s)G^{(2)}(s)$$
$$=\frac{-2}{\pi}\int_0^\infty \frac{1}{u}(2(1-\nu_1)f_1+uf_2)J_0(r_1 u)F(u)\,du=X_1 \tag{34}$$

$$I_1(r_1 s)A(s)+[4(1-\nu_1)I_1(r_1 s)-r_1 sI_0(r_1 s)]B(s)+K_1(r_1 s)C^{(2)}(s)-I_1(r_1 s)E^{(2)}(s)$$
$$-[4(1-\nu_2)K_1(r_1 s)+r_1 sK_0(r_1 s)]D^{(2)}(s)-[4(1-\nu_2)I_1(r_1 s)-r_1 sI_0(r_1 s)]G^{(2)}(s)$$
$$=\frac{-2}{\pi}\int_0^\infty \frac{1}{u}((2\nu_1-1)f_3+uf_4)J_1(r_1 u)F(u)\,du=X_2 \tag{35}$$

$$\mu_2\{C^{(2)}(s)[r_1 sK_0(r_1 s)+K_1(r_1 s)]-D^{(2)}(s)[(4-4\nu_2+r_1^2 s^2)K_1(r_1 s)+(3-2\nu_2)r_1 sK_0(r_1 s)]$$
$$+E^{(2)}(s)[r_1 sI_0(r_1 s)-I_1(r_1 s)]-G^{(2)}(s)[(4-4\nu_2+r_1^2 s^2)I_1(r_1 s)-(3-2\nu_2)r_1 sI_0(r_1 s)]\}$$
$$+\mu_1\{-A(s)[r_1 sI_0(r_1 s)-I_1(r_1 s)]+B(s)[(4-4\nu_2+r_1^2 s^2)I_1(r_1 s)-(3-2\nu_2)r_1 sI_0(r_1 s)]\}$$
$$=\frac{2}{\pi}r_1\mu_1\int_0^\infty F(u)\left[(-f_3+uf_4)J_0(r_1 u)+\{(1-2\nu_1)f_3-uf_4\}\frac{J_1(r_1 u)}{r_1 u}\right]du=X_3\mu_1 \tag{36}$$

$$\mu_2 s\{C^{(2)}(s)K_1(r_1 s)-D^{(2)}(s)[2(1-\nu_2)K_1(r_1 s)+r_1 sK_0(r_1 s)]-E^{(2)}(s)I_1(r_1 s)$$
$$-G^{(2)}(s)[2(1-\nu_2)I_1(r_1 s)-r_1 sI_0(r_1 s)]\}+\mu_1 s\{A(s)I_1(r_1 s)$$

$$+B(s)[2(1-\nu_1)I_1(r_1s)-r_1sI_0(r_1s)]\}=-\frac{2}{\pi}\mu_1\int_0^\infty uF(u)f_2J_1(r_1u)\,du=X_4\mu_1 \tag{37}$$

where, using the notation of Dhaliwal *et al.*,

$$f_1=\int_0^\infty \sin(sz)\,e^{-uz}\,dz=\frac{s}{(s^2+u^2)}$$

$$f_2=\int_0^\infty z\sin(sz)\,e^{-uz}\,dz=\frac{2su}{(s^2+u^2)^2}$$

$$f_3=\int_0^\infty \cos(sz)\,e^{-uz}\,dz=\frac{u}{(s^2+u^2)}$$

$$f_4=\int_0^\infty z\cos(sz)\,e^{-uz}\,dz=\frac{u^2-s^2}{(s^2+u^2)^2} \tag{38}$$

Imposing the boundary conditions given by eqns (28) along with eqns (13)–(16) and (18)–(21) and using the Fourier inversion theorem, we arrive at the following relations for $3\leqslant i\leqslant N-1$:

$$\begin{aligned}&-C^{(i-1)}(s)K_1(r_{i-1}s)+E^{(i-1)}(s)I_1(r_{i-1}s)+D^{(i-1)}(s)[4(1-\nu_{i-1})K_1(r_{i-1}s)+r_{i-1}sK_0(r_{i-1}s)]\\&\quad+G^{(i-1)}(s)[4(1-\nu_{i-1})I_1(r_{i-1}s)-r_{i-1}sI_0(r_{i-1}s)]\\&=-C^{(i)}(s)K_1(r_{i-1}s)+E^{(i)}(s)I_1(r_{i-1}s)+D^{(i)}(s)[4(1-\nu_{i-1})K_1(r_{i-1}s)+r_{i-1}sK_0(r_{i-1}s)]\\&\quad+G^{(i)}(s)[4(1-\nu_{i-1})I_1(r_{i-1}s)-r_{i-1}sI_0(r_{i-1}s)]\end{aligned} \tag{39}$$

$$\begin{aligned}&-C^{(i-1)}(s)K_0(r_{i-1}s)+D^{(i-1)}(s)r_{i-1}sK_1(r_{i-1}s)-E^{(i-1)}(s)I_0(r_{i-1}s)+G^{(i-1)}(s)r_{i-1}sI_1(r_{i-1}s)\\&\quad=-C^{(i)}(s)K_0(r_{i-1}s)+D^{(i)}(s)r_{i-1}sK_1(r_{i-1}s)-E^{(i)}(s)I_0(r_{i-1}s)+G^{(i)}(s)r_{i-1}sI_1(r_{i-1}s)\end{aligned} \tag{40}$$

$$\begin{aligned}&\frac{2\mu_{i-1}}{r_{i-1}}\{C^{(i-1)}(s)[r_{i-1}sK_0(r_{i-1}s)+K_1(r_{i-1}s)]-D^{(i-1)}(s)[(4-4\nu_{i-1}+r_{i-1}^2s^2)K_1(r_{i-1}s)\\&\quad+(3-2\nu_{i-1})r_{i-1}sK_0(r_{i-1}s)]+E^{(i-1)}(s)[r_{i-1}sI_0(r_{i-1}s)-I_1(r_{i-1}s)]\\&\quad-G^{(i-1)}(s)[(4-4\nu_{i-1}+r_{i-1}^2s^2)I_1(r_{i-1}s)-(3-2\nu_{i-1})r_{i-1}sI_0(r_{i-1}s)]\}\\&=\frac{2\mu_i}{r_{i-1}}\{C^{(i)}(s)[r_{i-1}sK_0(r_{i-1}s)+K_1(r_{i-1}s)]-D^{(i)}(s)[(4-4\nu_i+r_{i-1}^2s^2)K_1(r_{i-1}s)\\&\quad+(3-2\nu_{i-1})r_{i-1}sK_0(r_{i-1}s)]+E^{(i)}(s)[r_{i-1}sI_0(r_{i-1}s)-I_1(r_{i-1}s)]\\&\quad-G^{(i)}(s)[(4-4\nu_i+r_{i-1}^2s^2)I_1(r_{i-1}s)-(3-2\nu_i)r_{i-1}sI_0(r_{i-1}s)]\}\end{aligned} \tag{41}$$

$$\begin{aligned}&2\mu_{i-1}\{C^{(i-1)}(s)K_1(r_{i-1}s)-D^{(i-1)}(s)[2(1-\nu_{i-1})K_1(r_{i-1}s)+r_{i-1}sK_0(r_{i-1}s)]\\&\quad-E^{(i-1)}(s)I_1(r_{i-1}s)-G^{(i-1)}(s)[2(1-\nu_{i-1})I_1(r_{i-1}s)+r_{i-1}sI_0(r_{i-1}s)]\}\\&=2\mu_i\{C^{(i)}(s)K_1(r_{i-1}s)-D^{(i)}(s)[2(1-\nu_i)K_1(r_{i-1}s)+r_{i-1}sK_0(r_{i-1}s)]\\&\quad-E^{(i)}(s)I_1(r_{i-1}s)-G^{(i)}(s)[2(1-\nu_i)I_1(r_{i-1}s)+r_{i-1}sI_0(r_{i-1}s)]\}\end{aligned} \tag{42}$$

and at the last interface ($r=r_{N-1}$)

$$-C^{(N-1)}(s)K_1(r_{N-1}s)+E^{(N-1)}(s)I_1(r_{N-1}s)+D^{(N-1)}(s)[4(1-\nu_{N-1})K_1(r_{N-1}s)$$
$$+r_{N-1}sK_0(r_{N-1}s)]+G^{(N-1)}(s)[4(1-\nu_{N-1})I_1(r_{N-1}s)-r_{N-1}sI_0(r_{N-1}s)]$$
$$=C^{(N)}(s)K_1(r_{N-1}s)+D^{(N)}(s)[4(1-\nu_N)K_1(r_{N-1}s)+r_{N-1}sK_0(r_{N-1}s)] \quad (43)$$

$$-C^{(N-1)}(s)K_0(r_{N-1}s)+D^{(N-1)}(s)r_{N-1}sK_1(r_{N-1}s)-E^{(N-1)}(s)I_0(r_{N-1}s)$$
$$+G^{(N-1)}(s)r_{N-1}sI_1(r_{N-1}s)=-C^{(N)}(s)K_0(r_{N-1}s)+D^{(N)}(s)r_{N-1}sK_1(r_{N-1}s) \quad (44)$$

$$\frac{2\mu_{N-1}}{r_{N-1}}\{C^{(N-1)}(s)[r_{N-1}sK_0(r_{N-1}s)+K_1(r_{N-1}s)]$$
$$-D^{(N-1)}(s)[(4-4\nu_{N-1}+r_{N-1}^2s^2)K_1(r_{N-1}s)+(3-2\nu_{N-1})r_{N-1}sK_0(r_{N-1}s)]$$
$$+E^{(N-1)}(s)[r_{N-1}sI_0(r_{N-1}s)-I_1(r_{N-1}s)]$$
$$-G^{(N-1)}(s)[(4-4\nu_{N-1}+r_{N-1}^2s^2)I_1(r_{N-1}s)-(3-2\nu_{N-1})r_{N-1}sI_0(r_{N-1}s)]\}$$
$$=\frac{2\mu_N}{r_{N-1}}\{C^{(N)}(s)[r_{N-1}sK_0(r_{N-1}s)+K_1(r_{N-1}s)]$$
$$-D^{(N)}(s)[(4-4\nu_N+r_{N-1}^2s^2)K_1(r_{N-1}s)+(3-2\nu_N)r_{N-1}sK_0(r_{N-1}s)]\} \quad (45)$$

$$2\mu_{N-1}\{C^{(N-1)}(s)K_1(r_{N-1}s)-D^{(N-1)}(s)[2(1-\nu_{N-1})K_1(r_{N-1}s)+r_{N-1}sK_0(r_{N-1}s)]$$
$$-E^{(N-1)}(s)I_1(r_{N-1}s)-G^{(N-1)}(s)[2(1-\nu_{N-1})I_1(r_{N-1}s)+r_{N-1}sI_0(r_{N-1}s)]\}$$
$$=2\mu_N\{C^{(N)}(s)K_1(r_{N-1}s)-D^{(N)}(s)[2(1-\nu_N)K_1(r_{N-1}s)+r_{N-1}sK_0(r_{N-1}s)]\} \quad (46)$$

Equations (34)–(37) and (39)–(46) represent a system of $4(N-1)$ equations for the unknown functions $A(s)$, $B(s)$, $C^{(i)}(s)$, $D^{(i)}(s)$, $E^{(i)}(s)$, $F^{(i)}(s)$, $C^{(i)}(s)$, and $D^{(i)}(s)$ at each point in s-space. These equations may be solved by inverting the resulting matrix equation. It is then possible to write the functions $A(s)$ and $B(s)$ in the form

$$A(s)=A_1X_1+A_2X_2+A_3X_3+A_4X_4$$
$$B(s)=B_1X_1+B_2X_2+B_3X_3+B_4X_4 \quad (47)$$

where the coefficients A_i and B_i are determined by the matrix inverse.

Making use of eqn (47), we may then write the following expression in the form

$$[A(s)-2\nu_1B(s)]\sinh(st)-[st\cosh(st)-\sinh(st)]B(st)$$
$$=C_1(s,t)X_1+C_2(s,t)X_2+C_3(s,t)X_3+C_4(s,t)X_4 \quad (48)$$

where

$$C_1(s,t)=A_1\sinh(st)+B_1[(1-2\nu_1)\sinh(st)-st\cosh(st)]$$
$$C_2(s,t)=A_2\sinh(st)+B_2[(1-2\nu_1)\sinh(st)-st\cosh(st)]$$
$$C_3(s,t)=A_2\sinh(st)+B_2[(1-2\nu_1)\sinh(st)-st\cosh(st)]$$
$$C_4(s,t)=A_4\sinh(st)+B_4[(1-2\nu_1)\sinh(st)-st\cosh(st)] \quad (49)$$

Following the analysis of Dhaliwal *et al.* (1979), and making use of eqns (31) and (34), we find that the expression for X_1 can be written as

$$X_1 = \frac{-4(1-\nu_1)}{\pi}\int_0^{r_c} h(t)\,dt \int_0^{\infty} \frac{J_0(r_1 u)\sin(ut)\,du}{s^2+u^2} - \frac{4s}{\pi}\int_0^{r_c} h(t)\,dt \int_0^{\infty} \frac{u^2 J_0(r_1 u)\sin(ut)\,du}{(s^2+u^2)^2} \tag{50}$$

From Erdelyi (1954) we find that

$$I = \int_0^{\infty} \frac{J_0(r_1 u)\sin(ut)\,du}{s^2+u^2} = \frac{\sinh(st)K_0(r_1 s)}{s}, \quad t < b. \tag{51}$$

and

$$\int_0^{\infty} \frac{u^2 J_0(r_1 u)\sin(ut)\,du}{(s^2+u^2)^2} = I - s^2 \int_0^{\infty} \frac{J_0(r_1 u)\sin(ut)\,du}{(s^2+u^2)^2} \tag{52}$$

Differentiating both sides of eqn (51) with respect to s, we find that

$$\int_0^{\infty} \frac{J_0(r_1 u)\sin(ut)\,du}{(s^2+u^2)^2} = \frac{1}{2s}[\sinh(st)K_0(r_1 s) + r_1 s\sinh(st)K_1(r_1 s) - st\cosh(st)K_0(r_1 s)] \tag{53}$$

Substituting eqns (51)–(53) into eqn (50), we find that

$$X_1 = \frac{-2}{\pi}\int_0^{r_c} h(t)[(3-2\nu_1)\sinh(st)K_0(r_1 s) - r_1 s\sinh(st)K_1(r_1 s) + st\cosh(st)K_0(r_1 s)]\,dt \tag{54}$$

Following a similar procedure, we find that we may write

$$X_2 = -\frac{2}{\pi}(2\nu_1 - 1)\int_0^{r_c} h(t)\,dt \int_0^{\infty} \frac{uJ_1(r_1 u)\sin(ut)\,du}{s^2+u^2} - \frac{2}{\pi}\int_0^{r_c} h(t)\,dt \int_0^{\infty} \frac{u(u^2-s^2)J_1(r_1 u)\sinh(ut)\,du}{(s^2+u^2)^2} \tag{55}$$

The second term in eqn (55) may be rewritten as

$$\int_0^{\infty} \frac{u(u^2-s^2)J_1(r_1 u)\sinh(ut)\,du}{(s^2+u^2)^2} = \int_0^{\infty} \frac{uJ_1(r_1 u)\sin(ut)\,du}{s^2+u^2} - 2s^2\int_0^{\infty} \frac{uJ_1(r_1 u)\sin(ut)\,du}{(s^2+u^2)^2} \tag{56}$$

From Erdelyi (1954), we find that

$$\int_0^{\infty} \frac{uJ_1(r_1 u)\sin(ut)\,du}{s^2+u^2} = \sinh(st)K_1(r_1 s), \quad t < b. \tag{57}$$

Differentiating both sides of eqn (57), we obtain:

$$\int_0^\infty \frac{uJ_1(r_1u)\sin(ut)\,du}{(s^2+u^2)^2} = \frac{1}{2s^2}[\sinh(st)\{r_1sK_0(r_1s)+K_1(r_1s)\} - st\cosh(st)K_1(r_1s)] \tag{58}$$

Making use of eqns (57) and (58), we find that eqn (55) can be written as

$$X_2 = -\frac{2}{\pi}\int_0^{r_c} h(t)\{(2\nu_1-1)\sinh(st)K_1(r_1s) - [r_1s\sinh(st)K_0(r_1s) - st\cosh(st)K_1(r_1s)]\}\,dt \tag{59}$$

Using eqns (31), (36), (38), (52) and (57), we find that

$$X_3 = \frac{2}{\pi}\left[\int_0^{r_c} h(t)\{r_1s[r_1s\sinh(st)K_1(r_1s) - st\cosh(st)K_0(r_1s)] + (1-2\nu_1)\sinh(st)K_1(r_1s) - st\cosh(st)K_1(r_1s)\}\,dt\right] \tag{60}$$

Similarly, the expression for X_4 may be written as

$$X_4 = -\frac{4}{\pi}s\int_0^{r_c} h(t)\,dt\int_0^\infty \frac{u^3J_1(r_1u)\sin(ut)\,du}{(s^2+u^2)^2} \tag{61}$$

The second integral in eqn (61) can be written in the following form:

$$\int_0^{r_c} u\frac{u^2J_1(r_1u)\sin(ut)\,du}{(s^2+u^2)^2} = \int_0^\infty \frac{uJ_1(r_1u)\sin(ut)\,du}{s^2+u^2} - s^2\int_0^\infty \frac{uJ_1(r_1u)\sin(ut)\,du}{(s^2+u^2)^2} \tag{62}$$

so that

$$X_4 = -\frac{2}{\pi}\int_0^{r_c} h(t)[\sinh(st)K_1(r_1s) + st\cosh(st)K_1(r_1s) - r_1s\sinh(st)K_0(r_1s)]\,dt \tag{63}$$

By substituting eqns (49), (54), (59), (60) and (63) into eqn (33) we find the following relation

$$h(t) + \int_0^{r_c} h(u)K(u,t)\,du = -\frac{1}{\pi\mu_1}\int_0^t \frac{rp(r)\,dr}{\sqrt{t^2-r^2}}, \quad 0 < t < r_c, \tag{64}$$

where

$$\begin{aligned} K(u,t) = -\frac{4}{\pi}\int_0^\infty \{&[(3-2\nu_1)\sinh(us)K_0(r_1s) - r_1s\sinh(us)K_1(r_1s) \\ &+ us\cosh(r_1s)K_0(r_1s)]C_1(s,t) + [(2\nu_1-1)\sinh(us)K_1(r_1s) \\ &- \{r_1s\sinh(us)K_0(r_1s) - us\cosh(us)K_1(r_1s)\}]C_2(s,t) \\ &- [r_1^2s^2\sinh(us)K_1(r_1s) - (r_1s)(us)\cosh(us)K_0(r_1s) \\ &+ (1-2\nu_1)\sinh(us)K_1(r_1s) - us\cosh(us)K_1(r_1s)]C_3(s,t) \\ &+ [s\sinh(us)K_1(r_1s) + s(us)\cosh(us)K_1(r_1s) - s(r_1s)\sinh(us)K_0(r_1s)]C_4(s,t)\}\,ds \end{aligned} \tag{65}$$

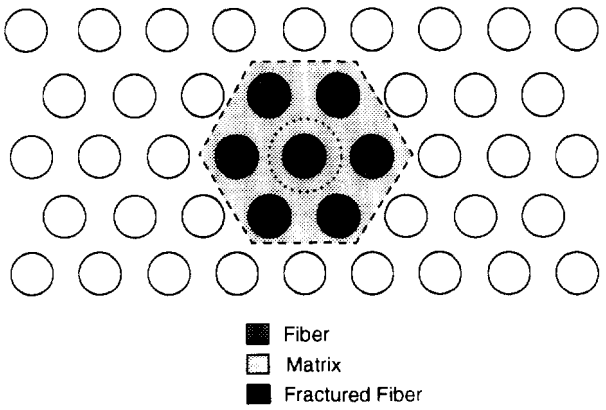

Fig. 2. Composite material having hexagonal packing which contains a single broken fiber. The shaded area is selected as a representative volume element for the analysis.

Equation (64) is a Fredholm integral equation of the second kind having a kernal given by eqn (65). This equation may be solved numerically for the unknown function $h(t)$.

5. REPRESENTATION OF THE BROKEN FIBER PROBLEM

To analyze a single fiber fracture in a unidirectional composite, we separate the problem into a near-field analysis and a far-field analysis. The total solution is then just the superposition of the far-field solution and the near-field solution. The far-field solution for a uniform strain applied in the fiber direction may be easily obtained in a manner such as that detailed by Pagano and Tandon (1988). In posing the near-field problem, we assume a fiber fracture has occurred in a composite with a hexagonal array of fibers, as shown in Fig. 2. The size of the crack is denoted by r_c, the size of the fiber by r_f, and the distance to the nearest adjacent fiber by r_2. Prior to the formation of the crack, load was carried by this region. The crack is opened by a pressure p_0 which is equal to the negative of the fiber stress determined from the far-field analysis such that the superposition of the near-field solution and the far-field solution produce a traction-free crack face. Following the suggestion of Carman (1993), we make the assumption that the fiber immediately adjacent to the fracture fiber may be represented by an annular ring of material (see Fig. 3). This assumption reduces the near-field problem to an axisymmetric one. While the point-wise stresses determined in such a manner are not the exact solution to the near-field problem, they do accurately depict the trends in the stress variations of interest. The inner radius of the fiber annular ring, r_2, is given by the distance to the adjacent fibers. The outer radius of the fiber annular ring, r_3, is determined from the global fiber volume fraction. For hexagonal packing, we have

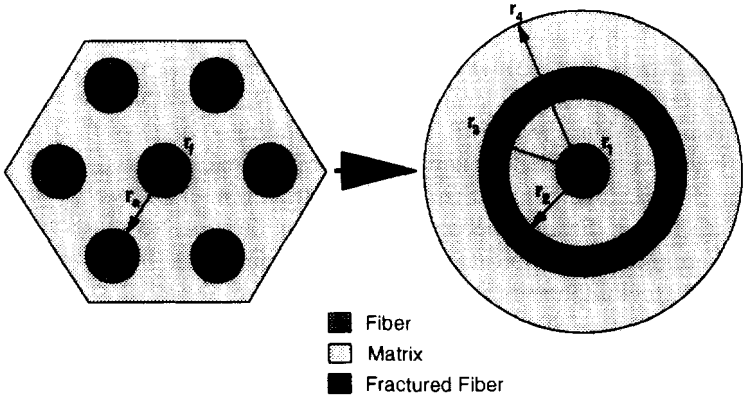

Fig. 3. Representation of the hexagonal arrangement as an axisymmetric one having the same fiber volume fraction.

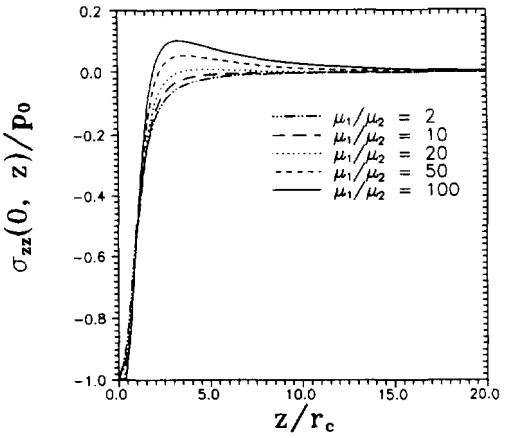

Fig. 4. Variation of the $\sigma_{zz}(0, z)$ stress (at the center of the broken fiber) as a function of distance above the crack plane for various fiber to matrix stiffness ratios.

$$r_3 = \sqrt{6r_1^2 + r_2^2}$$
$$r_4 = \frac{7r_1^2}{V_f} \tag{66}$$

In order to use the analysis developed previously in this paper, we allow the radius of the crack, r_c, to approach the radius of the fiber, r_1. Equation (64) is then solved numerically using the Nystrom method [Press *et al.* (1992)].

6. NUMERICAL RESULTS

To demonstrate the solution, a number of numerical studies were conducted. The first such study was to determine the effect of fiber to matrix stiffness ratio on the resulting stress state. To calculate the effective composite properties we use the following prescribed values

$$\nu_1 = \nu_2 = \nu_3 = \nu_4 = \nu_5 = 0.2$$
$$\mu_5 = \left[\frac{V_f}{\mu_1} + \frac{V_m}{\mu_2}\right] \tag{67}$$

While the use of isotropic properties to represent the composite could be questioned, this approximation is certainly not as severe as some of the others used in the model. First we look at the normal stress $\sigma_{zz}^{(1)}(0, z)$ (at the center of the broken fiber) for a 65% fiber volume fraction composite. This is shown graphically in Fig. 4. A number of interesting features are immediately noticeable. First of all, we see that for high values of the stiffness ratio, the normal stress becomes tensile before asymptotically approaching zero. Even more striking, however, is the distance over which the near-field stress remains compressive (the so-called ineffective length). This distance becomes smaller as the fiber to matrix stiffness ratio is increased. This is exactly the opposite trend from that predicted using a shear-lag analysis.

Of interest for making tensile strength predictions are the stress concentrations on the adjacent fibers and the axial distance over which this increased stress acts. Because there is a strain gradient as a function of r as well as z, it is not possible to speak of a single stress concentration value on the adjacent fiber. Rather this value depends upon position. To illustrate this, we will consider two different radial locations on the adjacent fiber ring: the inner edge of this ring ($r = r_2$) and the center of this ring, denoted $r_{1/2}$ and given by

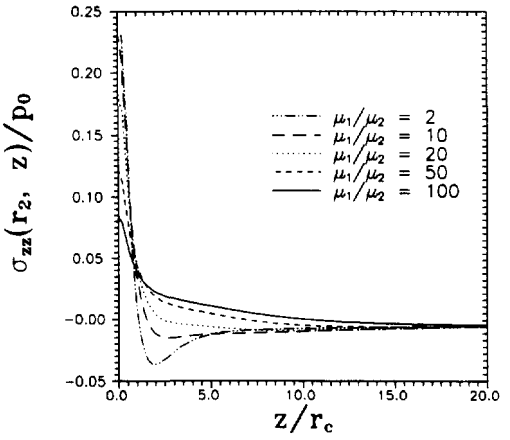

Fig. 5. Variation of the $\sigma_{zz}(r_2, z)$ stress (at the inside edge of the fiber annular ring) as a function of distance above the crack plane for various fiber to matrix stiffness ratios.

$$r_{1/2} = \tfrac{1}{2}(r_3 - r_2) + r_2 \tag{68}$$

Such a comparison is shown in Fig. 5 for the case of a 65% fiber volume fraction composite in which $\mu_1/\mu_2 = 20$. It will be noted that there is a great difference between the maximum stress values at these two locations. The maximum value at the inner edge is 0.183 while the maximum value at the center is 0.052. Another interesting feature is that the maximum stress concentration at the center of the adjacent ring does not occur in the plane of the crack. Rather, it is located at approximately 0.4 r_c above the plane of the crack. This is not surprising in view of the results given in Fig. 4, although it is a feature not predicted by the shear lag analysis. The maximum value of the stress concentration at the inner radius of the fiber ring does occur in the plane of the crack (for this particular selection of composite properties). To determine whether this was true in general, the stiffness ratio of the constituents was varied once again, and the resulting strain distributions plotted. The variation of the near-field stress as a function of axial distance from the crack plane at the inner edge of the fiber annular ring is shown in Fig. 5. Once again a fiber volume fraction of 65% was used. In all of the cases except one ($\mu_1/\mu_2 = 2$) the maximum stress concentration occurs in the plane of the crack. In this one case it occurs at 0.2 r_c above the crack plane. Two stiffness ratios considered, $\mu_1/\mu_2 = 2$ and $\mu_1/\mu_2 = 10$, give an almost identical value for the maximum stress concentration. Otherwise, there is a distinct trend: as the stiffness ratio is increased, the stress concentration at the inner radius of the fiber annular ring decreases.

The variation of the near-field stress as a function of distance from the crack plane for different stiffness ratios at the center of the fiber annular ring is illustrated in Fig. 6. Here

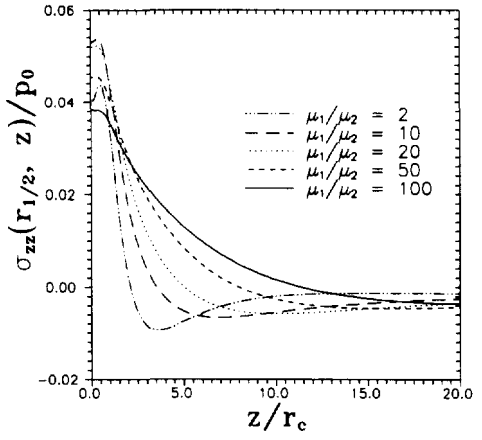

Fig. 6. Variation of the $\sigma_{zz}(r_{1/2}, z)$ stress (at the center of the fiber annular ring) as a function of distance above the crack plane for various fiber to matrix stiffness ratios.

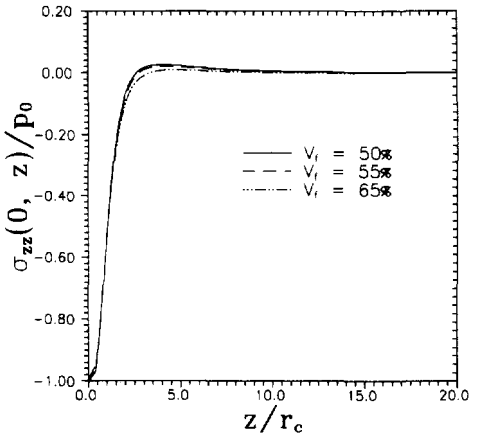

Fig. 7. Variation of the $\sigma_{zz}(0, z)$ stress (at the center of the broken fiber) as a function of distance above the crack plane for various fiber volume fractions.

the results follow an interesting pattern. As the stiffness is increased, the stress values increase initially and then decrease for higher stiffness values. However, all of these values are much less than would be predicted from a local load sharing rule. Hedgepeth and van Dyke's analysis predicts a stress concentration of 1.104 on the adjacent fiber, which is greater than the values obtained at the center by any of the cases studied. Such a result is not surprising in view of the amount of axial load being carried in the present model.

As a final example of application of the model, we consider the effect of fiber volume fraction on the stress state for composites in which $\mu_1/\mu_2 = 20$. Three different fiber volume fractions are considered: 50%, 55%, and 65%. First we consider the effect that those changes in fiber volume fraction have on the normal stress in the broken fiber. The results which are shown in Fig. 7 suggest that such changes have very little effect on the stress state in the broken fiber. However, if we consider the stress state at the center of the adjacent fiber ring as shown in Fig. 8 we see that changes in fiber volume fraction have a significant effect on the stress concentration seen here. The reason for these changes (the stress concentration goes up as the fiber volume fraction is increased) is easily understood physically if the geometry of the model is considered. As the fiber volume fraction is increased, the distance from the center of the unbroken fiber to the crack tip is decreased, leading to the larger stress concentration.

There is still one major point to be considered: the magnitude of the tensile stresses carried by the matrix, particularly at the crack tip. The radial variation of the normal

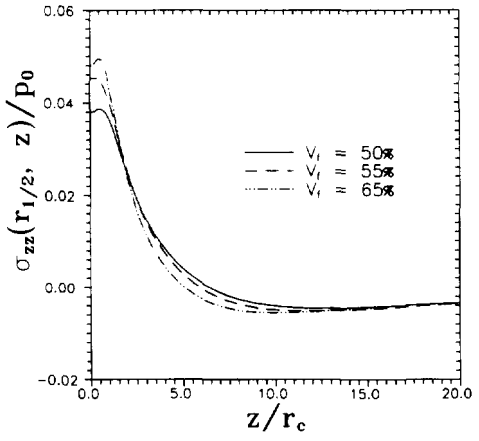

Fig. 8. Variation of the $\sigma_{zz}(r_{1/2}, z)$ stress (at the center of the fiber annular ring) as a function of distance above the crack plane for various fiber volume fractions.

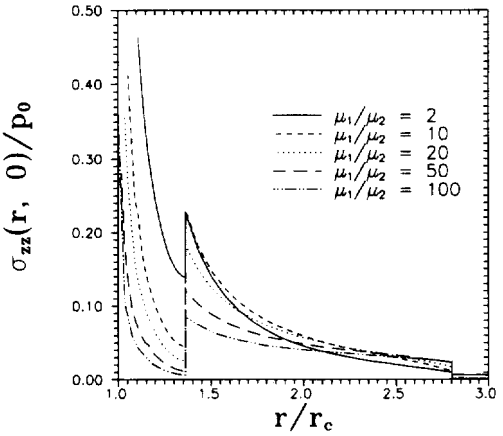

Fig. 9. Variation of the $\sigma_{zz}^{(i)}(r, 0)$ stress (in the plane of the crack) for the three inner concentric cylinders ($i = 2, 3, 4$).

stress, $\sigma_{zz}^{(i)}(r, 0)$ in the plane of the crack for the $i = 2, 3, 4$ cylinders is shown in Fig. 9 for a fiber volume fraction of 65%. The resulting stresses in the matrix adjacent to the crack tip are singular (as expected) with the power of the singularity increasing as the value of μ_1/μ_2 is increased. We would therefore expect some plasticity in the matrix, which would change the resulting stress state. This case has been recently studied using finite elements by Nedele and Wisnom (1994).

7. CONCLUSIONS AND CLOSING REMARKS

In this paper, an elasticity solution to the problem of a penny-shaped crack at the center on multiple concentric cylinders has been presented. The problem has been formulated as the solution to a system of dual integral equations which have been reducing to solving a Fredholm integral equation of the second kind. Once this solution has been obtained, it is then used in conjunction with an axisymmetric geometry approximation to examine the stress state around a broken fiber in a composite material. The solution suggests that other models such as shear lag may be missing important features of this stress state. In addition, the model may readily modified to include the effects of fiber coatings in the elastic stress concentrations. Once these stress concentrations (and the resulting ineffective lengths) have been determined, they may be incorporated into models such as that given by Batdorf (1982) for making tensile strength predictions of unidirectional composites.

However, there are still a number of limitations to the model. The most serious limitations are the assumptions of linear elasticity as well as the axisymmetric approximation. This severely distorts the local geometry. However, without the use of finite elements (which have difficulty modeling the singularity at the crack tip), this seems to be the best course of action at the present time. The are a number of ways that the present model could be improved. The assumption of isotropic constituents could be extended to allow the use of transversely isotropic constituents. Also, experimental evidence with model composite systems [Case *et al.* (1995)] suggests that in many cases a broken fiber is accompanied by a matrix crack which may extend to the adjacent fibers. This results in the adjacent fiber experiencing larger stress concentrations than when only a broken fiber is present. The present solution technique cannot be used for such a case (in which the crack is contained in two materials). Finally, there may also be a significant amount of plasticity at the crack tip which is not accounted for in the present analysis.

Acknowledgements—The authors gratefully acknowledge the support of the Air Force Office of Scientific Research under grant number FA9620-95-0217 and the National Science Foundation Science and Technology Center for High Performance Polymeric Adhesives and Composites under grant number DMR9120004.

REFERENCES

Atkinson, K. E. (1976). *A Survey of Numerical Methods for the Solution of Fredholm Integral Equations of the Second Kind*, S. I. A. M., Philadelphia.

Batdorf, S. B. (1982). Tensile strength of unidirectional reinforced composites—I. *J. Reinf. Plastics and Comp.* **1,** 153–176.

Carman, G. P., Lesko, J. J., and Reifsnider, K. L. (1993). Micromechanical analysis of fiber fracture. In *Composite Materials : Fatigue and Fracture*, Fourth Volume, ASTM STP 1156 (eds W. W. Stinchcomb and N. E. Ashbaugh) American Society for Testing and Materials, Philadelphia, pp. 430–452.

Case, S. W., Carman, G. P., Lesko, J. J., Fajardo, A. B., and Reifsnider, K. L. (1995). Fiber fracture in unidirectional composites. *J. Comp. Mat.* **29,** 208–228.

Collins, W. D. (1962). Some axially symmetric stress distributions in elastic solids containing penny-shaped cracks. I. Cracks in an infinite solid and a thick plate. *Proc. Roy. Soc. London A* **266,** 359–386.

Delves, L. M. and Mohamed, J. L. (1985). *Computational Methods for Integral Equations*, Cambridge University Press, Cambridge, U. K.

Dhaliwal, R. S., Singh, B. M., and Rokne, J. (1979). Penny-shaped crack in an infinite elastic cylinder bonded to an infinite elastic material surrounding it. *Int. J. Engng Sci.* **17,** 1245–1255.

Erdélyi, A. (ed.) (1954). *Tables of Integral Transforms*, Vol. 2, McGraw-Hill, New York.

Gao, Z. Reifsnider, K. L., and Carman, G. P. (1992). Strength prediction and optimization of composites with statistical fiber flaw distributions. *J. Comp. Mat.* **26,** 1678–1705.

Green, A. E. and Zerna, W. (1960). *Theoretical Elasticity*, Clarendon Press, Oxford.

Griffith, A. A. (1920). The phenomena of rupture and flow in solids. *Trans. Royal Soc. London*, **221,** 163–198.

Guidera, J. T. and Lardner, R. W. (1975). Penny-shaped cracks. *J. Elas.* **5,** 59–73.

Hedgepeth, J. M. and Van Dyke, P. (1967). Local stress concentration in imperfect filamentary composite materials. *J. Comp. Mat.* **1,** 294–309.

Keer, L. M. (1964). A class of non-symmetrical punch and crack problems. *Quart. J. Mech. and Appl. Math.* **17,** 423–436.

Lardner, R. W. and Tupholme, G. E. (1976). A note on arbitrarily loaded penny-shaped cracks in hexagonal crystals. *J. Elas.* **6,** 221–224.

Nedele and Wisnom. (1994). Stress concentration factors around a broken fibre in a unidirectional carbon fibre-reinforced epoxy. *Composites* **25,** 549–557.

Pagano, N. J., and Tandon, G. P. (1988). Elastic response of multi-directional coated-fiber composites. *Comp. Sci. and Tech.* **33,** 273–293.

Paris, P. C. and Sih, G. C. (1964). Stress analysis of cracks. *Fracture Toughness Testing and Its Applications*, ASTM STP 381, pp. 30–81.

Press, W. H., Teukolsky, S. A., Vetterling, W. T., and Flannery, B. P. (1992). *Numerical Recipes in FORTRAN: The Art of Scientific Computing*, Second Edition, Cambridge University Press, Cambridge, U. K.

Rosen, B. W. (1964). *Fiber Composite Materials*. American Society of Metals, Chapter 3, pp. 37–75.

Smith, F. W., Kobayashi, A. S. and Emery, A. F. (1967). Stress intensity factors for penny-shaped cracks. Part I—infinite solid. *J. Appl. Mech.* X, 947–952.

Sneddon, I. N. (1946). The distribution of stress in the neighborhood of a crack in an elastic solid. *Proc. Roy. Soc. London A* **187,** 229–260.

Sneddon, I. N. and Tait, R. J. (1963). The effect of a penny-shaped crack on the distribution of stress in a long circular cylinder. *Int. J. Engng Sci.* **1,** 391–409.

Whitney, J. M. and Drzal, L. T. (1987). Axisymmetric stress distribution around an isolated fiber fragment. *Toughened Composites*, ASTM STP 937 (ed. Norman J. Johnston) American Society for Testing and Materials, Philadelphia, pp. 179–196.